RESEARCH ON CONTROL STRATEGY OF POWER GRID SIMULATOR BASED ON PREDICTIVE CONTROL

Yong WANG[1], Chunmin SHI[1], Dingcheng GUO[1], Shuaishuai CHEN[2*], Zhihong ZHONG[2], Keli WANG[1]

With the increasing demand in urban power, new energy generation equipment has also been developed and applied on a large scale, and the demand for grid simulators used for grid-connected testing is also growing. The advantages of the three-phase four-bridge arm on the inverter side in the grid simulator are analyzed, and its topology is discussed. Through analyzing mathematical models in different coordinate systems, it is found that the three-sequence channels are not coupled in the αβγ coordinate system. This provides a good basis for the analysis of control strategies. Based on the model prediction control strategy, the four-bridge arm-type inverter is analyzed, and two types of control strategies: FCS-MPC and CCS-MPC are proposed and compared with the PR control strategy. The results show that CCS-MPC is more suitable for the control of three-phase four-bridge arm-type inverters.

Keywords: Three-phase four-bridge arm; Model predictive control; Split-sequence; Fault simulation

1. Introduction

With the continuous expansion of city scale and the continuous development of electric power technology, the demand for electric energy in cities is also continuously growing. To meet the demand for electricity in cities, the application of new energy generation technology is supported by technology and policy. Wind energy resources have the advantages of huge reserves, wide distribution and non-pollution. More and more countries are gradually attaching importance to the development of wind power. With the increasing number of wind power generation systems connected to the power grid, to ensure the stability of power grid operation, it is required that the wind power generation system can stabilize grid operation in the event of grid failure [1].

The main goal of grid simulator is to provide stable three-phase voltages and fault voltages under different faults, which can effectively provide a controllable and convenient fault testing environment for various new energy grid-

[1] Institute of Standards and Metrology, China Railway Research Institute Group Co, Beijing, China

[2]* Beijing Jiaotong University, Beijing, China, * Corresponding author's e-mail: 23126260@bjtu.edu.cn

connected devices. Therefore, research on improving the simulation accuracy and response speed of the grid simulator has become particularly important [2].

There have been many studies on grid simulators. Sun [3] designed an input-parallel-output-series (IPOS) grid simulator topology, which is suitable for the design of megawatt-level grid simulators. Wu [4] investigated the control strategy for the stability of output voltage in the case of unbalanced loads. Isakov et al. [5] adopted a topology based on series-coupled transformer banks, which greatly improved the simulation accuracy and response speed of high-power grid simulators. The control bandwidth of the high-power grid simulator system is greatly improved. Jiang et al. [6] controlled the positive-sequence component through virtual oscillator control (VOC) and suppressed the negative sequence component by designing virtual impedance and multi proportional resonance controller, thereby achieving more stable results. Sun et al. [7] integrated a higher-order sliding-mode observer (HOSMO) and finite-time feedback control technique for a four-legged inverter system using a nonlinear composite controller in the reference frame. We focus on the analysis of a four-bridge arm type grid simulator.

With the development of power electronic control theory, control strategies based on modern control theory have shown significant advantages in terms of intuitiveness and digital control implementation. Model predictive control (MPC) uses the mathematical model of the controlled object to implement the optimal control behavior through optimization principles. Due to its ability to introduce constraints, it has been widely studied and applied in power electronic control. There have been many studies and applications in power electronics control. Chen et al. [8] proposed a constrained model predictive control based on parallel neural network optimization, which is applied to PV grid-connected inverters to improve the grid-connected power quality of PV power generation. Fayyaz et al. [9] proposed the TP4LI model, which aims to predict and control switching frequency and higher voltage/current switching to reduce losses. Alladi et al. [10] proposed a model predictive control (MPC) for a four-legged power distribution static compensator (FL-DSTATCOM), which uses model predictive control (MPC) to compensate for power quality and reduce high neutral leg switching frequency of the FL-DSTATCOM. Bakeer et al. [11] described a new model-free predictive control (MFPC) approach for accurate voltage control of a four-leg voltage source inverter (4L-VSI). Gao [12] described the construction of a predictive model for a three-phase four-bridge-arm inverter Principle. Model predictive control is capable of accomplishing the target output with a short response time and is suitable for grid simulators to accomplish the simulation of the target situation in a short period of time [13-15].

Taking the three-phase four-bridge-arm type grid simulator as the research object, the control strategy combining the divisible-sequence coordinate transformation method and the model predictive control with the target as the output

voltage is adopted. This can improve the simulation accuracy and response speed on the premise of realizing the basic working condition simulation of the grid simulator, aiming to achieve the functions of the grid simulator with less computing power.

2. Three-Phase Four-Bridge Arm Topology Analysis

2.1 Topology Analysis

The control object is a three-phase four-bridge arm inverter, and its basic topology is shown in Fig. 1.

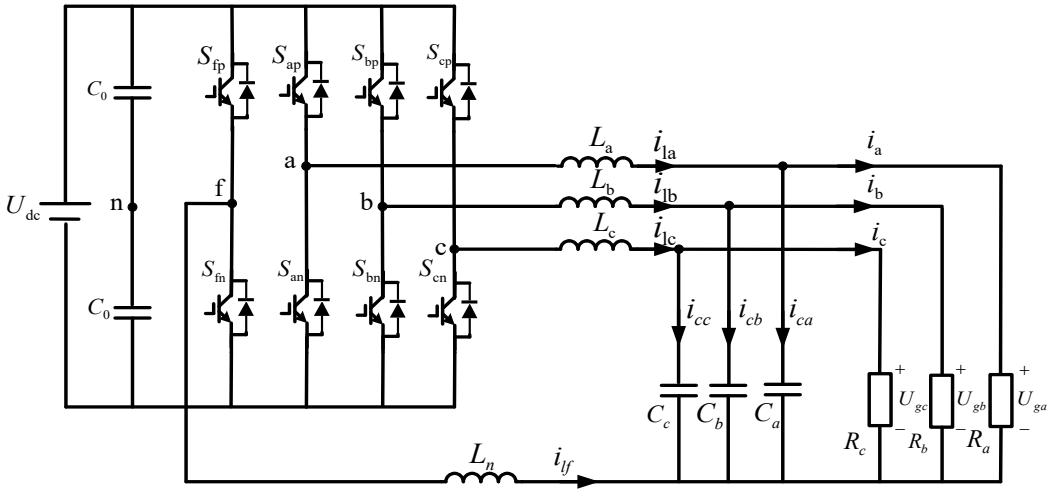

Fig. 1. Three-phase four-bridge-arm inverter circuit topology

As shown in Fig. 1, the main circuit topology consists of four bridge arms, each with two switches totaling eight switches. Three bridge arm filter parts and loads A, B and C are stacked to output a controllable three-phase voltage. Bridge arm F is the fourth bridge arm, and its voltage output point f is connected to the neutral point of the three-phase bridge arm load. Capacitor Co is the input filter capacitor with the same structure and size, and Udc is the voltage of DC side. The filtering link is LC filtering, and La, Lb, Lc are the filter inductors of each phase. Ln is the neutral line inductor, and Ca, Cb, and Cc are the filter capacitors of each phase, respectively. ila, ilb, ilc are the inductance currents of each phase. ilf is the neutral line current, and ica, icb, and icc are the capacitance current of each phase.

Since there are two switches in each bridge arm, there are two states, and the midpoint voltage is different in the two operating states. Let Ux (x=a, b, c) denote the value of the midpoint voltage of the bridge arm with respect to the ground, which can be obtained as follows:

$$Ux=\begin{cases}Udc & \text{Upper tube on}\\ 0 & \text{Upper tube closed}\end{cases},\ x=a,b,c,f \tag{1}$$

Let Sx denote the state of the upper bridge arm switch, Sx=1 means on, and Sx=0 means off. The state of the lower bridge arm switch is in the opposite of it, and Eq. (1) can be expressed as follows:

$$U_x=S_xU_{dc},x=a,b,c,f \tag{2}$$

S_{af}, S_{bf} and S_{cf} are the difference between the switching signals S_x (x=a, b, c) of the three ABC bridge arms and the switching signals Sf of the fourth bridge arm, respectively. Since there are 8 switches in 4 bridge arms, there are 16 conditions of the voltage vector.

Let d_x (x=a, b, c) be the duty cycle corresponding to the switching signal S_x. According to the topology of Fig. 1 and Kirchhoff's law, the relationship between the parameters can be obtained as follows:

$$\begin{bmatrix}d_a\\ d_b\\ d_c\end{bmatrix}U_{dc}=L\frac{d}{dt}\begin{bmatrix}i_{la}\\ i_{lb}\\ i_{lc}\end{bmatrix}+\begin{bmatrix}u_{ca}\\ u_{cb}\\ u_{cc}\end{bmatrix}-L_n\frac{d}{dt}\begin{bmatrix}i_{lf}\\ i_{lf}\\ i_{lf}\end{bmatrix} \tag{3}$$

$$C\frac{d}{dt}\begin{bmatrix}u_{ca}\\ u_{cb}\\ u_{cc}\end{bmatrix}=\begin{bmatrix}i_{la}\\ i_{lb}\\ i_{lc}\end{bmatrix}-\begin{bmatrix}i_a\\ i_b\\ i_c\end{bmatrix} \tag{4}$$

2.2 αβγ Coordinate System Model

It can be seen that the topology in dqo coordinate system has coupling quantities and is not suitable for analysis. Therefore, the analysis is carried out in the αβγ coordinate system. The mathematical model of three-phase four-bridge-arm inverter with midline inductance in the αβγ coordinate system can be obtained through the Clark transform with Eqs. (3) and (4). The equal amplitude Clark transform matrix is as follows:

$$T_{abc/\alpha\beta\gamma}=\begin{bmatrix}1 & -\frac{1}{2} & -\frac{1}{2}\\ 0 & \frac{\sqrt{3}}{2} & -\frac{\sqrt{3}}{2}\\ \frac{1}{2} & \frac{1}{2} & \frac{1}{2}\end{bmatrix} \tag{5}$$

Implementing the above transformations to Eqs. (3) and (4), the mathematical model in the αβγ coordinate system can be obtained as follows:

$$U_{dc}\begin{bmatrix} d_\alpha \\ d_\beta \\ d_\gamma \end{bmatrix} = \begin{bmatrix} L & 0 & 0 \\ 0 & L & 0 \\ 0 & 0 & L+3L_n \end{bmatrix} \frac{d}{dt}\begin{bmatrix} i_{l\alpha} \\ i_{l\beta} \\ i_{l\gamma} \end{bmatrix} + \begin{bmatrix} u_{c\alpha} \\ u_{c\beta} \\ u_{c\gamma} \end{bmatrix} \tag{6}$$

$$C\frac{d}{dt}\begin{bmatrix} u_{c\alpha} \\ u_{c\beta} \\ u_{c\gamma} \end{bmatrix} = \begin{bmatrix} i_{l\alpha} \\ i_{l\beta} \\ i_{l\gamma} \end{bmatrix} - \begin{bmatrix} i_\alpha \\ i_\beta \\ i_\gamma \end{bmatrix} \tag{7}$$

From Eqs. (6) and (7), the equivalent model in the αβγ coordinate system is shown in Fig. 2.

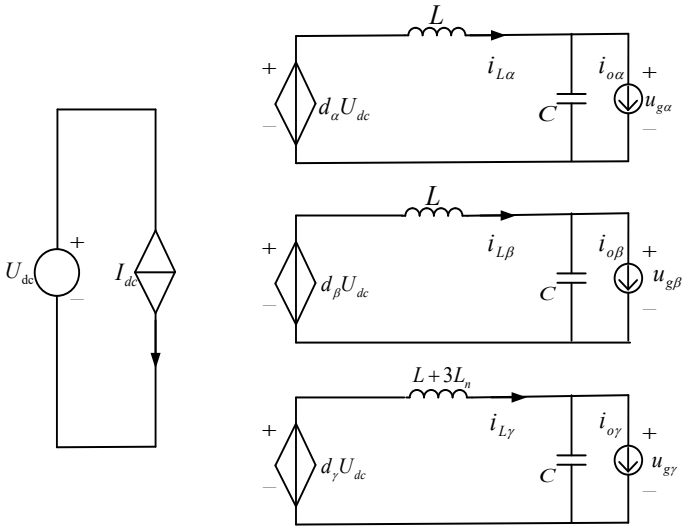

Fig. 2. Equivalent model of three-phase four-bridge arm inverter in the αβγ coordinate system

From Fig. 2, α, β, γ channels in the equivalent model are independent to each other, without coupling in the αβγ coordinate system. Compared with the original equivalent model of the four-bridge inverter with centerline inductance and the equivalent model in the dqo coordinate system, the voltage of each channel in the equivalent model can be controlled directly without decoupling. The design of the controller is simpler. Analyzing the symmetrical components of the equivalent model, the rotational transformation of each sequence component can be obtained as follows:

$$\begin{bmatrix} u_{\alpha p} \\ u_{\beta p} \\ u_{\gamma p} \end{bmatrix} = \begin{bmatrix} U_p \sin(\omega t + \varphi_0) \\ U_p \sin(\omega t + \varphi_0 - \frac{\pi}{2}) \\ 0 \end{bmatrix} \tag{8}$$

$$\begin{bmatrix} u_{\alpha n} \\ u_{\beta n} \\ u_{\gamma n} \end{bmatrix} = \begin{bmatrix} U_n \sin(\omega t + \varphi_0) \\ U_n \sin(\omega t + \varphi_0 + \frac{\pi}{2}) \\ 0 \end{bmatrix} \tag{9}$$

$$\begin{bmatrix} u_{\alpha 0} \\ u_{\beta 0} \\ u_{\gamma 0} \end{bmatrix} = \begin{bmatrix} 0 \\ 0 \\ U_0 \sin(\omega t + \varphi_0) \end{bmatrix} \tag{10}$$

3. Model Predictive Control

3.1 Three-Phase Four-Bridge Arm Prediction Model

The basic principle of model predictive control is based on the relationship between the parameters of the control object. In the field of inverters, control design is usually based on its state space equations. Due to the lack of coupling between the three-phase channels in the αβγ coordinate system, the control of the phases can be carried out in a simple way. Due to the lack of coupling between the three-phase channels in the α - β - γ coordinate system, phase control can be performed in a very simple manner. To simplify the subsequent analysis, the voltage and current vectors used are defined as follows:

$$U_d = [U_{afd} \quad U_{bfd} \quad U_{cfd}]^T \tag{11}$$

$$U = [U_{af} \quad U_{bf} \quad U_{cf}]^T \tag{12}$$

$$U_o = [U_{ga} \quad U_{gb} \quad U_{gc}]^T \tag{13}$$

$$i = [i_{la} \quad i_{lb} \quad i_{lc}]^T \tag{14}$$

$$i_o = [i_a \quad i_b \quad i_c]^T \tag{15}$$

where Eq. (11) is the discrete voltage vector at each moment at switch closure, and Eq. (12) is the continuous average vector obtained after calculating the switch duty cycle. Eq. (11) is used as the bridge arm output voltage variable in FCS-MPC, and Eq. (12) is used as the bridge arm output voltage variable in CCS-MPC.

According to the equivalent model analysis in Chapter 2, the models of the three channels in the αβγ coordinate system are consistent, and only the equivalent inductance value of the γ channel is different. Therefore, the equivalent model in the αβγ coordinate system is used to establish the prediction model.

According to Eqs. (6), (7) and Fig. 2, the state space equation of the single-channel equivalent model in the αβγ coordinate system can be obtained as follows:

$$\begin{bmatrix} \dot{u}_c \\ \dot{i}_L \end{bmatrix} = \frac{d}{dt}\begin{bmatrix} u_c \\ i_L \end{bmatrix} = \begin{bmatrix} 0 & 1/C \\ -1/L & 0 \end{bmatrix}\begin{bmatrix} u_c \\ i_L \end{bmatrix} + \begin{bmatrix} 0 & -1/C \\ 1/L & 0 \end{bmatrix}\begin{bmatrix} U_{in} \\ i_o \end{bmatrix} \tag{16}$$

where the equivalent inductance of the γ channel is $L+3L_n$. From the principle of predictive control, it is necessary to ensure that the solution of the discretized state equation at the sampling moment is the same as that of the original state equation in the premise of the above continuous equations to be discretized accurately. Therefore, T is the switching period, and the matrix I is the unitary matrix. The coefficient matrix can be obtained by simplifying the corresponding discrete-time based state space equations, i.e., the prediction model:

$$\begin{bmatrix} U_o(k+1) \\ i(k+1) \end{bmatrix} = G\begin{bmatrix} U_o(k) \\ i(k) \end{bmatrix} + H\begin{bmatrix} U_{in}(k) \\ i_o(k) \end{bmatrix} \tag{17}$$

$$G = \begin{bmatrix} G_{11} & G_{12} \\ G_{21} & G_{22} \end{bmatrix} = \begin{bmatrix} \cos(\frac{T}{\sqrt{LC}}) & \frac{\sqrt{L}}{\sqrt{C}}\sin(\frac{T}{\sqrt{LC}}) \\ \frac{-\sqrt{C}}{\sqrt{L}}\sin(\frac{T}{\sqrt{LC}}) & \cos(\frac{T}{\sqrt{LC}}) \end{bmatrix} \tag{18}$$

$$H = \begin{bmatrix} H_{11} & H_{12} \\ H_{21} & H_{22} \end{bmatrix} = \begin{bmatrix} 1-\cos(\frac{T}{\sqrt{LC}}) & \frac{-\sqrt{L}}{\sqrt{C}}\sin(\frac{T}{\sqrt{LC}}) \\ \frac{\sqrt{C}}{\sqrt{L}}\sin(\frac{T}{\sqrt{LC}}) & 1-\cos(\frac{T}{\sqrt{LC}}) \end{bmatrix} \tag{19}$$

3.2 Finite Set Predictive Control (FCS-MPC)

The control method of FCS-MPC is to list all switching states, obtain the outputs of all possible cases, and design a cost function based on the set optimization objective to obtain the optimal switching cases and adopt this signal control system. Based on the analysis of the three-phase four-bridge arm topology in Section II, it can be learned that there are a total of 8 pairs of switches, i.e., 16 possible switching states, which correspond to the output voltage vector of the bridge arm. The control in the αβγ coordinate system is shown in Table 1.

Table 1

Switching State and Voltage Vector Table

Switching status	Vectors	α-β-γ coordinate system		
(Sa. Sb. Sc. Sf)	***Ui***	U_α	U_β	U_γ
0000	$\boldsymbol{U_1}$	0	0	0
0001	$\boldsymbol{U_2}$	0	0	$-U_{dc}$
0010	$\boldsymbol{U_3}$	$-U_{dc}/3$	$-U_{dc}/\sqrt{3}$	$-U_{dc}/3$
0011	$\boldsymbol{U_4}$	$-U_{dc}/3$	$-U_{dc}/\sqrt{3}$	$-2U_{dc}/3$
0100	$\boldsymbol{U_5}$	$-U_{dc}/3$	$U_{dc}/\sqrt{3}$	$U_{dc}/3$
0101	$\boldsymbol{U_6}$	$-U_{dc}/3$	$U_{dc}/\sqrt{3}$	$-2U_{dc}/3$
0110	$\boldsymbol{U_7}$	$-2U_{dc}/3$	0	$2U_{dc}/3$

0111	$\boldsymbol{U_8}$	$-2U_{dc}/3$	0	$-U_{dc}/3$
1000	$\boldsymbol{U_9}$	$2U_{dc}/3$	0	$U_{dc}/3$
1001	$\boldsymbol{U_{10}}$	$2U_{dc}/3$	0	$-2U_{dc}/3$
1010	$\boldsymbol{U_{11}}$	$U_{dc}/3$	$-U_{dc}/\sqrt{3}$	$2U_{dc}/3$
1011	$\boldsymbol{U_{12}}$	$U_{dc}/3$	$-U_{dc}/\sqrt{3}$	$-U_{dc}/3$
1100	$\boldsymbol{U_{13}}$	$U_{dc}/3$	$U_{dc}/\sqrt{3}$	$2U_{dc}/3$
1101	$\boldsymbol{U_{14}}$	$U_{dc}/3$	$U_{dc}/\sqrt{3}$	$-U_{dc}/3$
1110	$\boldsymbol{U_{15}}$	0	0	U_{dc}
1111	$\boldsymbol{U_{16}}$	0	0	0

The optimization is to solve the bridge arm output voltage vector $U_d(k)$ for the condition where the error between the output voltage and the reference voltage is minimized. At the next moment of the vector element $U_d(k+1)$, the output voltage of the bridge arm at moment k+1 is taken as the next moment of the system input. Therefore, according to Eq. (18), $U_o(k+1)$ can be obtained in a recursive form as shown in Eq. (20).

$$U_o(k+1) = G_{11}U_o(k) + G_{12}i(k) + H_{11}U_d(k) + H_{12}i_o(k) \tag{20}$$

According to Eq. (20), it can be seen that the output voltage Uo(k+1) at the next moment can be obtained from Uo(k), i(k), io(k), and Ud(k) at the current moment. Where Uo(k), i(k), and io(k) can be obtained by sampling, and Ud(k) is the 16 switching voltage vectors shown in Table 1. All cases of the predicted output voltage Uo(k+1) at the next moment are obtained.

The control objective of the inverter in the grid simulator is the voltage of the output target, and the optimization objective is that the predicted voltage is equal to the reference voltage. In the design of cost functions, it is generally common to directly use the sum of squared differences between prediction and reference, as shown in Eq. (21).

$$g = \sum (U_{refx}(k+1) - U_{ox}(k+1))^2, x = a,b,c \tag{21}$$

Based on the above inference, the FCS-MPC flowchart can be obtained as shown in Fig. 3.

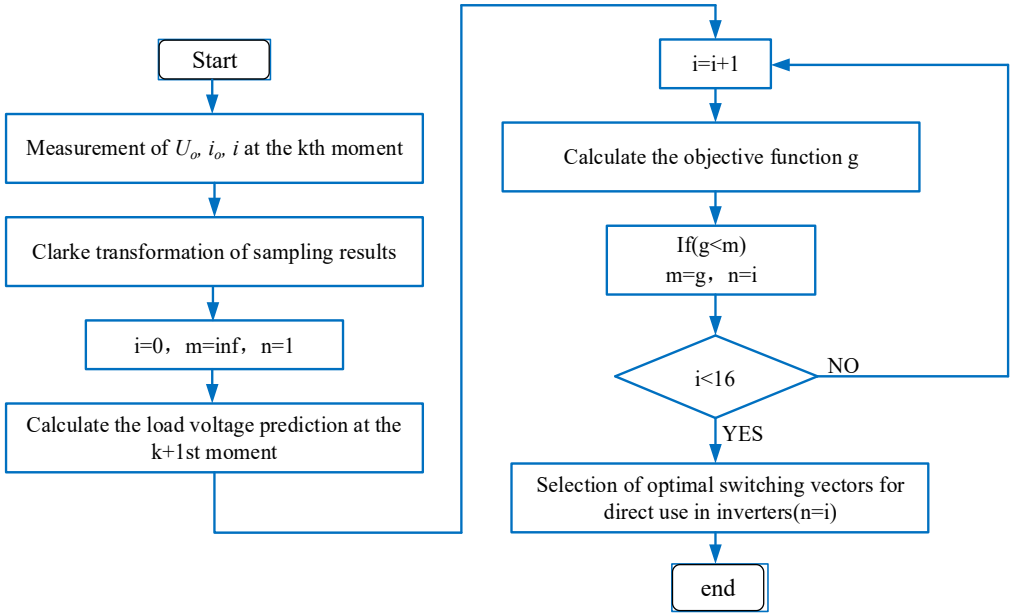

Fig. 3. FCS-MPC Voltage Control Algorithm Flowchart

3.3 Continuous Set Predictive Control (CCS-MPC)

In CCS-MPC, U(k) is the average of Ud(k) over one switching cycle, which is a continuous vector. It is impossible to obtain the optimal situation by predicting all possible scenarios, so other methods are needed to solve it. Compared with FCS-MPC, this scheme ultimately obtains a continuous voltage vector, which is then modulated by PWM to control the switching signals.

Similar to FCS-MPC, the predicted recursive equations for Uo(k+1) and i(k+1) can be obtained according to Eq. (20)'s as shown in Eqs. (22) and (23).

$$U_o(k+1) = G_{11}U_o(k) + G_{12}i(k) + H_{11}U(k) + H_{12}i_o(k) \tag{22}$$

$$i(k+1) = G_{21}U_o(k) + G_{22}i(k) + H_{21}U(k) + H_{22}i_o(k) \tag{23}$$

Based on the common cost function design, the cost function g under one-step continuous set predictive control can be obtained according to Eq. (21):

$$\begin{aligned} g &= H_{11}^2U(k)^2 - 2H_{11}(U_{oref}(k+1) - G_{11}U_o(k) - G_{12}i(k) - H_{12}i_o(k))^2U(k) \\ &= aU(k)^2 + bU(k) \end{aligned} \tag{24}$$

According to Eq. (24), the cost function is a quadratic function of the output voltage U(k) of the bridge arm at moment k. Since a=H11^2>0, the optimal point value of this cost function, i.e., the minimum value point Uopt(k), can be determined by the Maximum Theorem as follows:

$$Uopt(k) = -\frac{b}{2a} = \frac{U_{oref}(k+1) - G_{11}Uo(k) - G_{12}i(k) - H_{12}io(k)}{H_{11}} \tag{25}$$

The optimal input voltage Uopt(k) at time k obtained from the above solution is the component of the voltage vector to be synthesized on the channel (α, β or γ) at the current moment of the αβγ-3DSVM modulation link. The αβγ-3DSVM is similar to the PWM modulation mechanism, which adjusts the switching duty ratio according to the target voltage to achieve the ideal voltage output, which is not described here. Based on the above content single-channel one-step CCS-MPC flow is shown in Fig. 4.

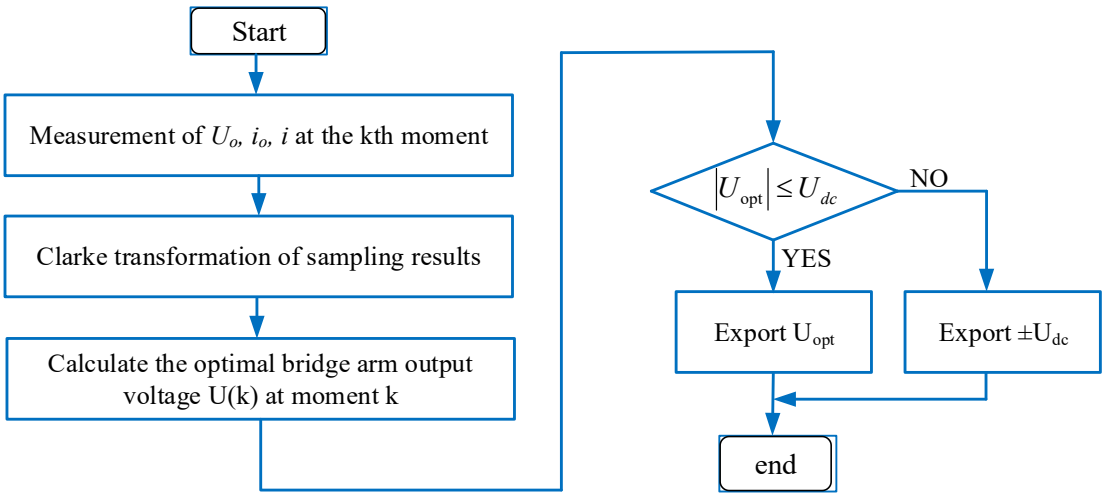

Fig. 4. Flowchart of One-step CCS-MPC Voltage Control Algorithm

One-step control prediction considers the optimal situation in a cycle. There is still a gap for the subsequent two to more steps, which cannot maintain the optimal situation for a long time. However, to verify two and more steps in the predictive control, the output effect is close to one-step and the computational complexity is large, so that only one-step prediction is analyzed.

3.4 Simulation Comparison

Based on simulation verifying the correctness of the finite-set predictive control method and the accuracy of the predictive model, the effectiveness of the predictive control scheme is demonstrated by comparing the PR control strategy with the three types of modeled predictive control strategies under different situations. The switching frequency selected in the simulation is 10kHz, and the sampling frequency used in predictive control is 12kHz. Under balanced load, the RMS value of each phase voltage is 220V; the rated power with load is 2kW, and the voltage on the dc side is 700V. The main simulation parameters are shown in Table 2.

Table 2

Simulation Parameter Setting

Parameters	Values
Control period T	0.1ms
DC Side Voltage Udc	350V
Reference voltage Uref	220V
Filter Inductors L	2.5mH
Filter capacitor C	80μF
Output Voltage Frequency fs	50Hz

The steady state performance is the stability of the output voltage under unbalanced load; the transient performance is to observe the response speed of the output voltage under load switching and fault simulation. When testing the steady state performance, the load situation is three-phase asymmetrical impedance, each with 10Ω resistance, B-phase series 0.3mH inductance, C-phase series 10μF capacitance, to observe the three-phase voltage THD situation.

Voltage dip refers to the transient process in which the voltage of the power grid suddenly drops to 10%~90% of the rated voltage within a short period of time (usually 0.5 cycles to 1 minute), and then recovers automatically. When testing the transient response, the load switching is the sudden unloading of phase A, and the three-phase voltage fluctuation is observed. Fault simulation is to change the reference voltage of phase A to 80% of the original voltage, and observe the response speed of phase A voltage.

3.4.1 Single-Phase Load Switching Simulation Results

The waveforms of the output voltages of the four schemes under single-phase load switching are shown in Fig. 5.

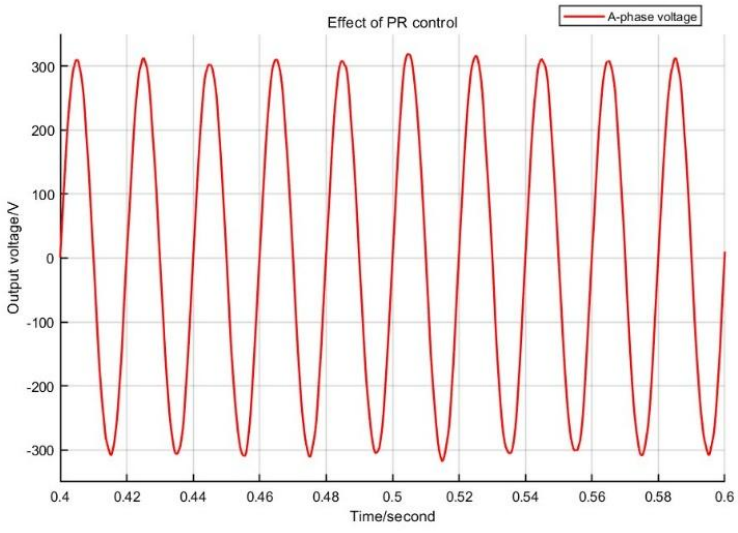

(a) PR control effect

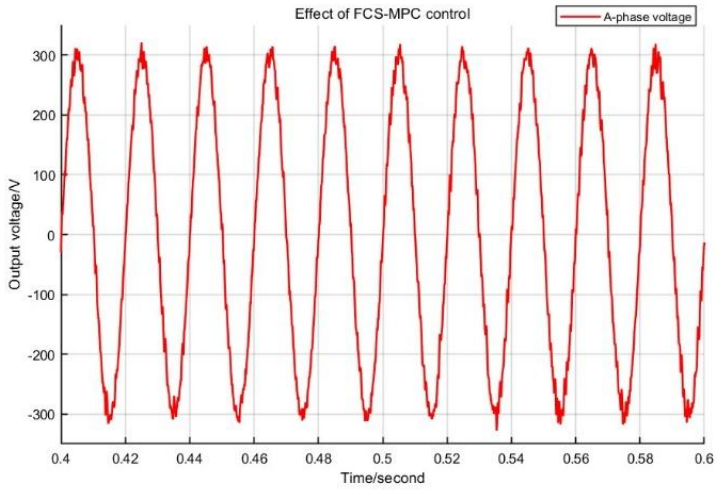

(b) FCS-MPC control effect

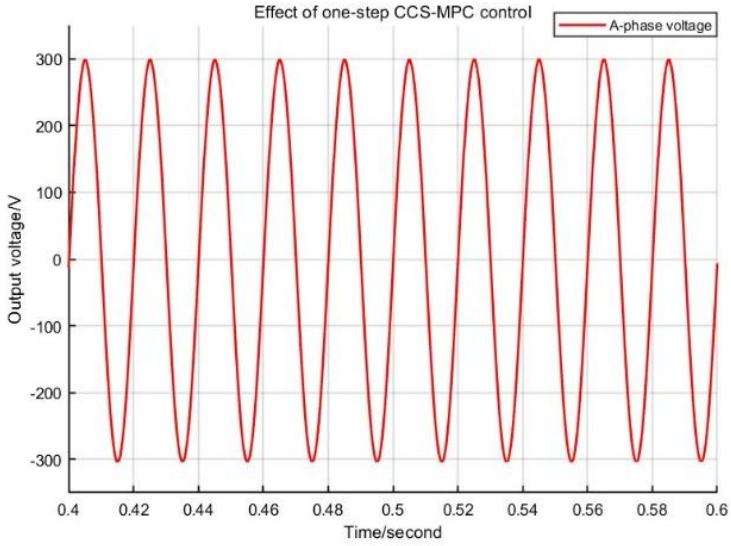

(c) One-step CCS-MPC control effect

Fig. 5 Output voltage waveform under single-phase load switching

The THDs of the output voltages of the four schemes are shown in Table 3. It can be seen that the steady state effect of the continuous-set predictive control is slightly better than that of the PR control. However, the two-step continuous-set predictive control has a certain degree of increase in voltage magnitude error, which is considered as an error in load current and reference voltage estimation.

Table 3

Simulation results of four control schemes

Type of control	amplitude error	THD
PR control	0.23V	0.16%
	0.26V	0.18%
	0.25V	0.19%
FCS-MPC	1.70V	5.47%
	4.60V	4.98%
	3.60V	5.86%
One-step CCS-MPC	0.20V	0.16%
	0.20V	0.14%
	0.10V	0.13%

3.4.2 Simulation Results of Single-Phase Voltage Surge Faults

The waveforms of the output voltages of the four schemes under single-phase load switching are shown in Fig. 6. The output voltage response speeds of the four schemes are shown in Table 4. The response speeds of the three predictive controls are significantly faster than that of the PR control.

Table 4

Simulation results of four control schemes

Control types	Responsive time
PR control	128ms
FCS-MPC	14ms
One-step CCS-MPC	17ms

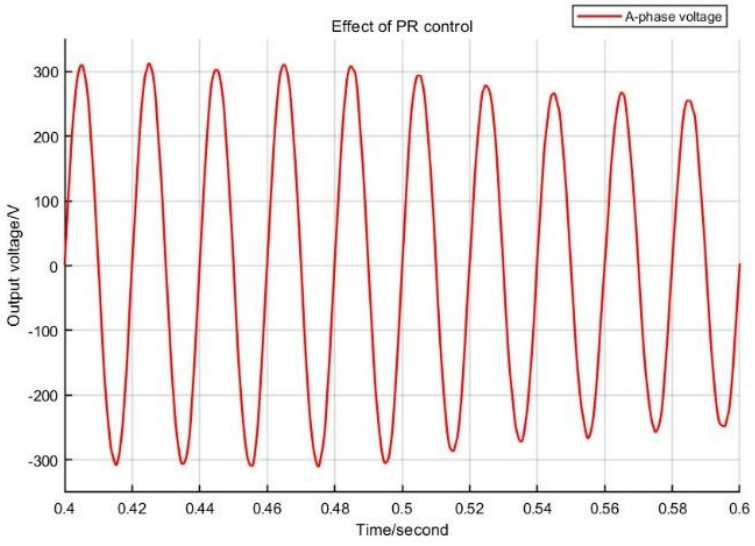

(a) PR control effect

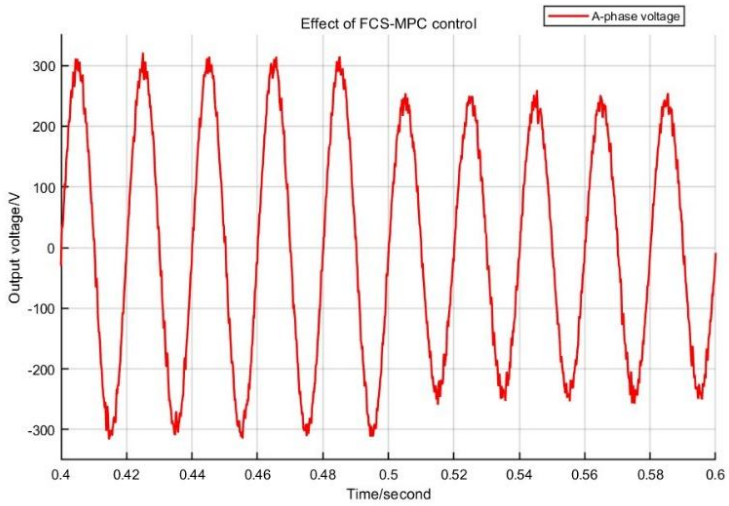

(b) FCS-MPC control effect

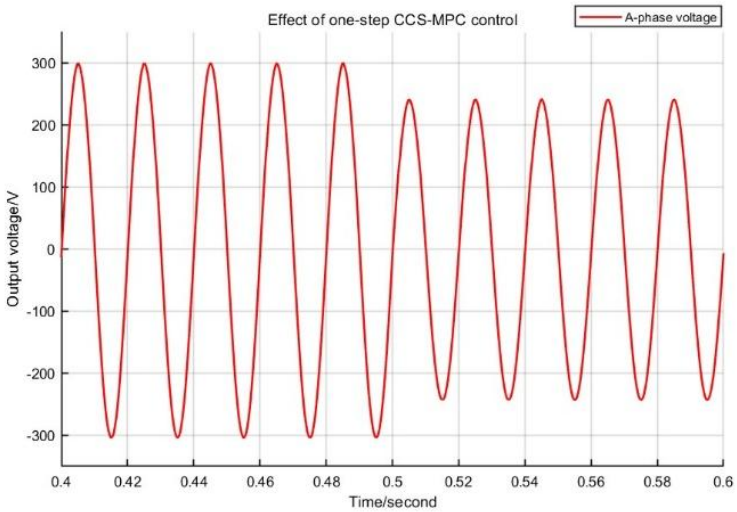

(c) One-step CCS-MPC control effect

Fig. 6. Output voltage waveforms for single-phase voltage surge fault simulation cases

4. Conclusion

The advantages of using a three-phase four-bridge-arm on the inverter side of the grid simulator are analyzed. First, its topology is examined, and through the analysis of its mathematical model in different coordinate systems, it is demonstrated that the three-sequence channels are not coupled in the αβγ coordinate system, making it suitable for the analysis of the control strategy. Then the four-bridge-arm type of inverter is analyzed by using the model predictive control strategy, and the two types of control strategies: FCS-MPC and CCS-MPC are

derived. The simulation results of FCS-MPC and CCS-MPC are compared and analyzed with the PR control strategy. The analysis concludes that one step of CCS-MPC is more suitable for the control of three-phase four-bridge arm-type inverters. Future work will focus on optimizing this scheme.

Acknowledgement

Project of Distributed Energy Storage System Testing Technology based on Grid Simulation (2023YJ284).

REFERENCES

[1] *Tong, C., Zhang, H., Wang, Z., Liu, Y., & Li, X.* "Refined Urban Grid Simulation Planning Based on Low Carbon Goal Achievement", Applied Mathematics and Nonlinear Sciences, **vol. 9**, no. 1, 2024. 2024. https://doi.org/10.2478/amns.2023.2.01287

[2] *Mazzarino, P. R., Macii, A., Bottaccioli, L., & Patti, E.* "A Multi-Agent Framework for Smart Grid Simulations: Strategies for power-to-heat flexibility management in residential context", Sustainable Energy, Grids and Networks, **vol. 34**, 2023, pp. 101072. https://doi.org/10.1016/j.segan.2023.101072

[3] *Sun, Y.* "Research on Topology and Control Strategy of 35kV Medium Voltage Megawatt Grid Simulator", Hefei University of Technology, 2022. DOI: 10.27101/d.cnki.ghfgu.2022.001550

[4] *Wu, L.H.* "Research on Control Strategy of Three-phase Inverter under Asymmertrical Load", Harbin Engineering University, 2021. DOI: 10.27060/d.cnki.ghbcu.2022.002344

[5] *Isakov, I., Rapaić, M., Vekić, M., Grabić, S., & Todorović, I.* "Simulator of Decentralized Control Strategies in Electrical Grids", 2021 20th International Symposium INFOTEH-JAHORINA (INFOTEH), East Sarajevo, Bosnia and Herzegovina, IEEE, 2021, pp. 1-5. Doi: 10.1109/INFOTEH51037.2021.9400668

[6] *Jiang, H., Pan, H., & Shang, B.* "An individual sequencing control strategy for three-phase four-leg inverter under unbalanced loads", Energy Reports, **vol. 9**, no. S10, 2023, pp. 256-266. https://doi.org/10.1016/j.egyr.2023.05.079

[7] *Sun, Y., Zhang, C., & Su, Z. G.* "Disturbance observer-based composite voltage synchronisation control of three-phase four-leg inverter under load variation", International Journal of Control, **vol. 95**, no. 6, 2022, pp. 1645-1657. https://doi.org/10.1080/00207179.2020.1867324

[8] *Chen, Q.H., Luo, X.R., Zhang, L.Y.* "Constrained Model Predictive Control for Three-Phase Four-Leg Grid-Tied Inverter", Power System Technology, **vol. 42**, no. 2, 2018, pp. 555-563. Doi: 10.13335/j.1000-3673.pst.2017.1810

[9] *Fayyaz, M. M., Syed, I. M., Meng, Y., & Aman, M. N.* "Comprehensive Predictive Control Model for a Three-Phase Four-Legged Inverter", Energies, **vol. 16**, no. 6, 2023, pp. 2650. https://doi.org/10.3390/en16062650

[10] *Alladi, P. K., Ganjikunta, S. K., & Dharmavarapu, S.* "Model predictive control with technique for order of preference by similarity to ideal solution method for four leg distribution static compensator to improve power quality and reduce switching frequency", International Transactions on Electrical Energy Systems, **vol. 31**, no. 1, 2021, pp. e12688. https://doi.org/10.1002/2050-7038.12688

[11] *Bakeer, A., Abid, A., Albalawi, H. A., Magdy, G., Chub, A., & Zaid, S. A.* "Robust Operation of Four-Leg Voltage Source Inverter Using Model-Free Predictive Control", Journal of Electrical Engineering & Technology, 2024, pp. 1-18. https://doi.org/10.1007/s42835-024-02018-z

[12] *Gao, J.X.* "Research on sequence decomposition predictive control strategy of three-phase four-leg inverter", Harbin Institute of Technology, 2022. Doi: 10.27061/d.cnki.ghgdu.2022.003871

[13] *Qin, G., Chen, Q., & Zhang, L.* "Finite control set model predictive control based on three-phase four-leg grid-connected inverters", 2020 35th Youth Academic Annual Conference of Chinese Association of Automation (YAC), Zhanjiang, China, IEEE, 2020, pp. 680-684. Doi: 10.1109/YAC51587.2020.9337710

[14] *Rao, R., & Hou, S.* "Model Predictive Control for Cascaded Multilevel Inverter Based on Lyapunov Function", 2019 IEEE Innovative Smart Grid Technologies - Asia (ISGT Asia), Chengdu, China, IEEE, 2019, pp. 2314-2318. Doi: 10.1109/ISGT-Asia.2019.8881554

[15] *Feng, Z., Cao, W., Rui, T., Hu, C., & Yin, Z.* "A Model-Free Predictive Control Method for Grid-Tied Inverter Based on Discrete Space Vector", 2021 IEEE International Conference on Predictive Control of Electrical Drives and Power Electronics (PRECEDE), Jinan, China, IEEE, 2021, pp. 634-639. Doi: 10.1109/PRECEDE51386.2021.9680938